Water **2014**, *6*, 271-300; doi:10.3390/w6020271

OPEN ACCESS

water

ISSN 2073-4441

www.mdpi.com/journal/water

Article

Nationwide Digital Terrain Models for Topographic Depression Modelling in Detection of Flood Detention Areas

Jenni-Mari Vesakoski [1,*], Petteri Alho [1,2], Juha Hyyppä [3], Markus Holopainen [4], Claude Flener [1] and Hannu Hyyppä [2,5]

[1] Department of Geography and Geology, University of Turku, Turku FI-20014, Finland; E-Mails: petteri.alho@utu.fi (P.A.); claude.flener@utu.fi (C.F.)

[2] Department of Real Estate, Planning and Geoinformatics, School of Engineering, Aalto University, Aalto FI-00076, Finland; E-Mail: hannu.hyyppa@aalto.fi

[3] Department of Remote Sensing and Photogrammetry, Finnish Geodetic Institute, Masala FI-02431, Finland; E-Mail: juha.hyyppa@fgi.fi

[4] Department of Forest Sciences, University of Helsinki, Helsinki FI-00014, Finland; E-Mail: markus.holopainen@helsinki.fi

[5] Civil Engineering and Building Services, Helsinki Metropolia University of Applied Sciences, Helsinki FI-00079, Finland

* Author to whom correspondence should be addressed; E-Mail: jmeves@utu.fi; Tel.: +358-2-333-5669.

Received: 19 November 2013; in revised form: 15 January 2014 / Accepted: 22 January 2014 / Published: 28 January 2014

Abstract: Topographic depressions have an important role in hydrological processes as they affect the water balance and runoff response of a watershed. Nevertheless, research has focused in detail neither on the effects of acquisition and processing methods nor on the effects of resolution of nationwide grid digital terrain models (DTMs) on topographic depressions or the hydrological impacts of depressions. Here, we quantify the variation of hydrological depression variables between DTMs with different acquisition methods, processing methods and grid sizes based on nationwide 25 m × 25 m and 10 m × 10 m DTMs and 2 m × 2 m ALS-DTM in Finland. The variables considered are the mean depth of the depression, the number of its pixels, and its area and volume. Shallow and single-pixel depressions and the effect of mean filtering on ALS-DTM were also studied. Quantitative methods and error models were employed. In our study, the depression variables were dependent on the scale, area and acquisition method. When the depths of depression pixels were compared with the most accurate DTM, the maximum errors were

found to create the largest differences between DTMs and hence dominated the amount and statistical distribution of the depth error. On the whole, the ability of a DTM to accurately represent depressions varied uniquely according to each depression, although DTMs also displayed certain typical characteristics. Thus, a DTM's higher resolution is no guarantee of a more accurate representation of topographic depressions, even though acquisition and processing methods have an important bearing on the accuracy.

Keywords: ALS; DTM; nationwide DEM; grid size; topographic depression; flood detention

1. Introduction

Spatial information is widely used in fluvial applications, the potential of which is increasing owing to technological advances in topographic data acquisition. Laser scanning in particular has enabled more accurate data gathering with decreased horizontal and vertical error and better availability of detailed spatial data. For example, airborne laser scanning (ALS) [1–5], ALS systems for bathymetric measurements [6], fixed-position terrestrial laser scanning (TLS) and mobile laser scanning (MLS), such as boat- and cart-based mobile mapping systems (BoMMS/CartMMS) [7,8], have shown new potential in fluvial research.

The acquisition method [9–12] and data processing method, such as grid size resampling [13,14], of the elevation dataset impact on the accuracy of represented terrain derivatives. Furthermore, horizontal [10–16] and vertical accuracy [10,17], terrain relief [13], algorithms used for terrain derivative delineation and data structure affect the accuracy of a digital terrain model (DTM) [10]. Grid DTMs, which store elevation values in a regular matrix of pixels, are commonly used in hydrologic analyses. The resolution, acquisition method and processing methods of a grid mainly determine its error as a level of accuracy. The effects of the acquisition method and grid size of a DTM on hydrologically interesting terrain derivatives, such as river network and watershed representation, slope and aspect, specific catchment areas and CTI-values (Compound Topographic Index), have been studied [10–12,18]. Additionally, the impact of vertical errors of DTMs on terrain derivatives has been examined [10,17] as well as the impact of DTMs on hydrologic modelling [15,16,19] and flood simulation [3,14,18]. The suitability of a DTM for terrain analysis has also been examined. For example, Oksanen [20] focused on developing a three-step framework for exploring the suitability of a DEM for terrain analyses; visualisation tools for detecting morphological gross errors [21], exploratory spatial analysis of DTM error [22] and DEM error propagation analysis [23,24]. The last-mentioned step focused on the results of error propagation analysis of slope, aspect and drainage basin delineation.

Because topographic depressions have an important role in hydrological processes as they affect the water balance and runoff response of a watershed [25], they are used in flood risk management. Nevertheless, research has not focused in detail on the effects of acquisition and processing methods and resolution of a grid DTM on topographic depressions or the hydrological impacts of depressions. Few studies have considered the effect of DTM grid size resampling on geometric attributes of depressions [25–27]. To be more precise, Zandbergen [26] resampled 6 m grid size laser scanning based DTM, Abedini *et al*. [25] resampled 3 mm grid size laser scanning based DTMs covering

15 runoff plots, and Yang and Chu [27] resampled 5 mm grid size small laboratory surfaces and field plots based on laser scanning and also watershed surfaces based on 30 m USGS-DTMs (U.S. Geological Survey). Special attention has been paid to the total volume of depressions [13,28–30]. Research has also been performed on the effects of DTM grid size and the effects of a grid matrix placement in relation to terrain on spurious depressions in DTMs [31] and also the effects of DTM vertical error on depressions [32]. Furthermore, the potential of high-resolution DTMs to represent linear anthropogenic features, such as depressions, and the use of these for more accurate flow pattern modelling in human modified landscapes [4] has been examined. Additionally, research concerning the effects of depressions on hydrologic models [5], the effects of the terrain slope [33], the effects of surface roughness [34,35] on depressions and also the impacts of grid size on hydrologic connectivity has been performed.

There have been no studies, as far as the authors are aware, concerning the characteristics of nationwide DTMs in topographic depression detection. Recently, many countries have conducted nationwide ALS surveys, principally for DTM purposes (e.g., the Netherlands, Switzerland, Denmark, Finland, Sweden, Austria, Germany and the USA). For example, Denmark produced a digital elevation model in 2006 and 2007 with national average point accuracy of 5.9 cm and point density of 1.6 m [36], and Sweden's new national elevation model will be available by 2015 and will have 2 m grid spacing with mean vertical error of 0.5 m or less [37]. The National Land Survey of Finland (NLS) began to gather new ALS-DTM data in 2008 that are planned to cover the whole country by 2019 [38]. Initially, the collection concentrated on flood-prone areas. After the scanning of spring 2013, the total coverage was approximately 235,000 km^2 [39]. Thus, there is a growing need for better knowledge of the suitability of nationwide elevation datasets for different study fields. All in all, detailed comparison between accessible nationwide ALS-DTMs with different grid sizes and DTMs that represent more conventional acquisition methods, such as photogrammetric methods, is needed.

The objective of this study is to quantify the variation of hydrological depression variables between nationwide DTMs with different acquisition methods, processing methods and grid sizes. Our depression detection is based on nationwide 25 m × 25 m and 10 m × 10 m DTMs and 2 m × 2 m ALS-DTM produced by NLS of Finland. The depression variables considered are the mean depth of the depression, the number of its pixels, and its area and volume. Furthermore, shallow and single-pixel depressions are examined and also the effect of mean filtering on high-resolution ALS-DTM. The results are compared with both field reference VRS-GNSS data (Virtual Reference Stations, Global Navigation Satellite Systems) and the most accurate DTM verified with the aforementioned field reference. Moreover, the differences of depression pixel depths in relation to the most accurate DTM are determined and the effect of resolution on the detention areas for flooding is evaluated.

2. Background

Topographic depressions are part of a large framework of flood protection to control water movement in a specific time scale (Figure 1). These effects cause changes in the shape and size of hydrographs, runoff volume and time [5,25,40]. Thus, the aforementioned influences are brought about by changes in water detention and direct surface runoff and are mainly achieved by adding, storing and restoring detention and absorption areas for water on a watershed scale.

Figure 1. Topographic depressions in the field (left) and in a grid digital terrain model (DTM) (middle and right). Depressions can be simple or complex. Simple depressions have one pour point (PP) and complex ones have more than one pour point of which one is the actual pour point (APP) and the others are shared pour points (SPP) [40].

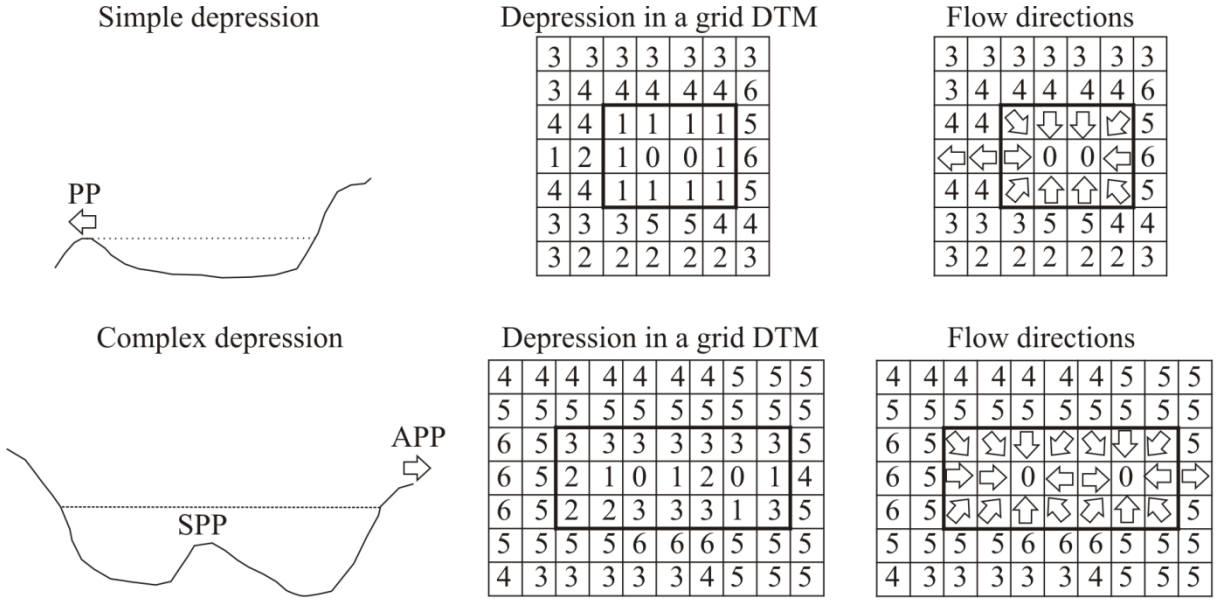

Topographic depression is defined as local minima of elevation values that have no downslope flow paths [41] (Figure 1). Consequently, depressions are removed from a grid DTM prior to hydrologic analyses that are based on automated simulation of surface runoff [41–43]. These analyses require hydrologically connected flow networks, in which the flow to the actual pour point of the watershed is not prevented.

There are two main conventions in depression preprocessing [44]. In the first one, depressions in DTMs are real landscape features, and thus, methods do not modify them. According to the second convention, depressions are spurious features caused by errors in DTM. These can be divided into methods that process the whole DTM and methods that process only the problematic areas. These methods that process only specific areas are commonly used in hydrology, and comprise filling, breaching and combination methods (Figure 2) [42]. For example, Jenson and Domingue [41] developed a filling method that is now implemented widely in commercial software products [1], whereas several studies [1,45,46] have developed filling methods that are more suitable for large data processing than the aforementioned method. A breaching method known as the *phenomenon-based approach*, in which main flow paths are formed, was developed by Rieger [47]. These flow paths form continuous paths from the deepest part of a depression to the actual pour point of the area studied (Figure 2). A combination method called the Impact Reduction Approach (IRA) was developed by Lindsay and Creed [48]. This method selects either the filling or the breaching method based on the impact factor (IF) that indicates the amount of change in a DTM necessary for hydrologic correction of the area processed. The method requiring the smallest change is chosen.

Figure 2. Main principles of depression preprocessing methods. Depressions are caused by underestimation of elevation values following filling methods that raise elevation values of depression pixels. With the breaching methods, however, depressions are caused by overestimation of elevation values which form topographic features that block water flow.

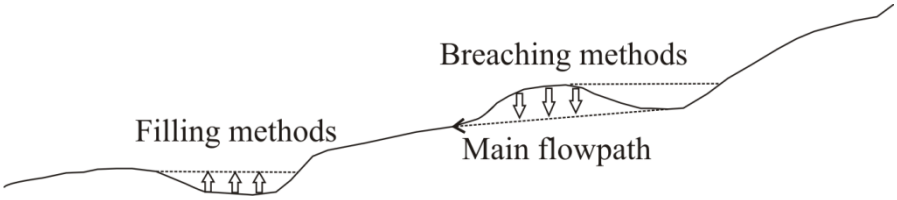

Depressions in a DTM are a combination of spurious and real terrain features. The separation of these depression types is essential because of the impacts of real topographic depressions on environmental processes such as watershed hydrology [49]. The development of a depression classifier as a selective removal method is emphasised in low and smooth terrain, when accurate ALS-models are used in which vertical error is near to the elevation differences of neighbouring pixels [26] or when DTMs are used whose grid sizes are too large for detailed topography representation [31]. The availability of more accurate DTMs that contain large amounts of depressions owed to LiDAR (Light Detection and Ranging) technology also underlines the need for a classifier. For example, Liu and Wang [2] classified modelled depressions from high-resolution ALS-DTM based on their spatial variables. Zandbergen [32] focused on the effects of vertical accuracies of DTMs on the probability of modelled depressions being actual landscape features. Lindsay and Creed [49] represented five approaches for distinguishing real and spurious depressions from DTMs: ground inspection, examination of source data, classification, and knowledge-based and modelling approaches.

3. Study Areas

Our study areas are the Lehmäjoki River (166 km^2), the Nenättömänluoma River (107 km^2) and the upper reaches of the Kainastonjoki River (87 km^2) whose watersheds are sub-basin areas (SBAs) of the Kyrönjoki River watershed (Figure 3). The Kyrönjoki River watershed is located in the western part of Finland and its main river bed drains into the Gulf of Bothnia. It mainly drains on a relatively flat terrain, if the slopes of the three main tributaries of the Jalasjoki, Kauhajoki and Seinäjoki Rivers are greater than the very gentle slopes of the main river bed [50]. The catchment area is 4923 km^2 in size and the proportion of lakes is small (1.23%). The principles of flood risk management were applied to this flood-prone watershed in the 1960s. Consequently, extensive flood protection initiatives (1966–2004) were executed. Also, flood risks have been evaluated and the significant flood risk areas are listed by the Ministry of Agriculture and Forestry [51]. Two of these are situated in the Kyrönjoki River watershed.

In this study, the watersheds were delineated by using techniques that involve the integration of a specified vector hydrography layer [52], in which the stream network produced by the Finnish Environment Institute was used. This stream network was added to the DTM by subtracting elevation values of the river network from the unprocessed DTM. Thus, the pixels of the river network were lowered. The flow directions, flow accumulation values, pour points and watersheds were delineated to this processed DTM; additionally, the unprocessed DTM was cut by a watershed polygon.

Figure 3. The watershed of Kyrönjoki River and the SBAs studied.

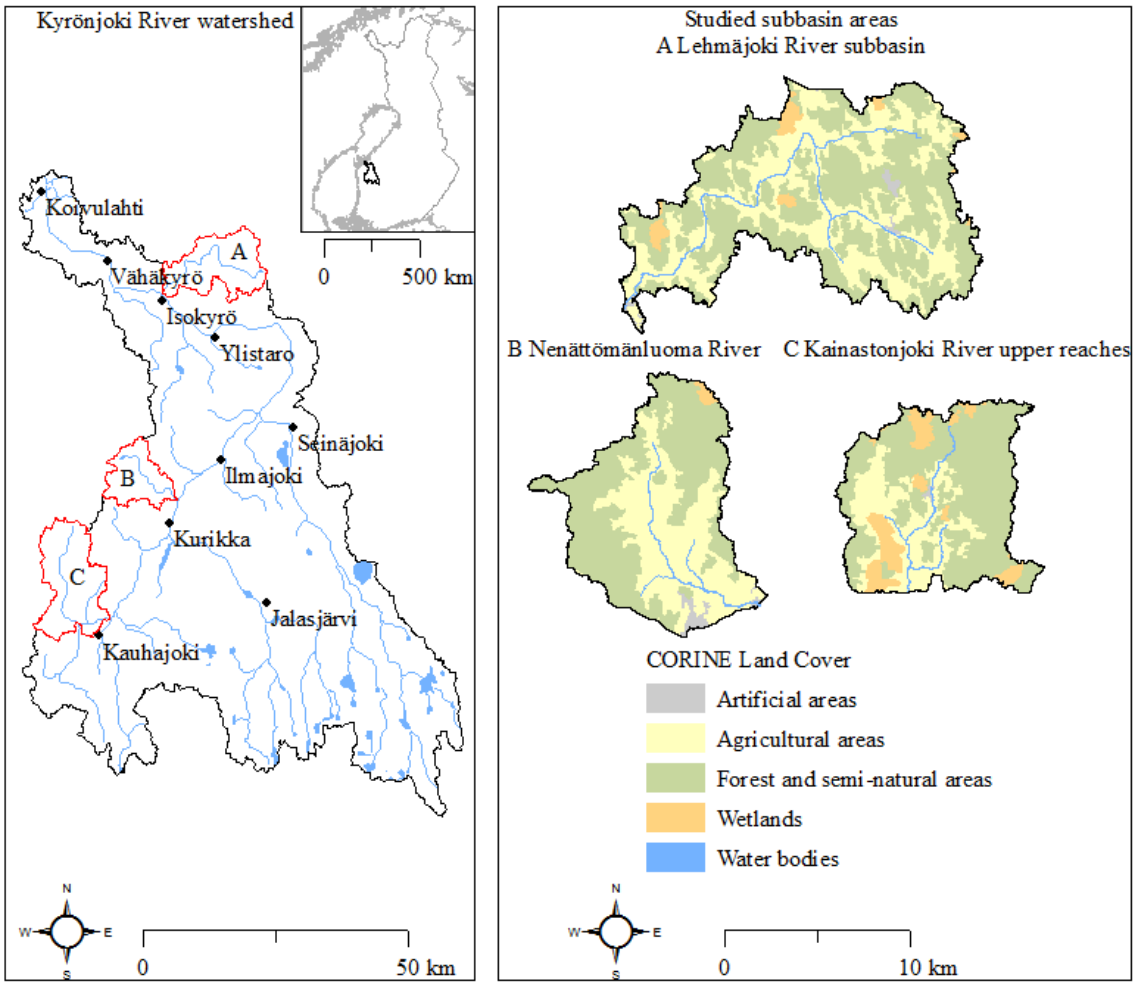

4. Materials and Methods

4.1. Field Survey Data

Field data were collected to provide reference data for the accuracy delineation of the DTMs. We gathered 10,022 reference points from depressions in the Lehmäjoki River SBA with VRS-GNSS with average horizontal standard deviation of 0.023 m and average vertical standard deviation of 0.04 m. The satisfactory measure of DOP-value (Dilution of Precision) as PDOP-value (Position Dilution of Precision) of gathered points was set at ≤5. PDOP is a figure that expresses the relationship between the error of GPS position and the error of satellite position. Thus, it illustrates the positional measurement accuracy and the smaller the value the more accurate the point gathered.

4.2. Laser Scanning Data

Recently, several countries have performed nationwide ALS surveys primary for DTM purposes. In our study, ALS-DTM with 2 m grid size was used (Figure 4). This DTM is based on the ALS point cloud that covers terrain with at least 0.5 points per 1 m^2 (later ALS-DTM2) with accuracy of 0.3 m [53,54]. The vertical point accuracy of the DTM is 0.15 m and horizontal accuracy is 0.6 m in an unambiguous terrain surface. The ground points were selected from the point cloud and checked

with TerraScan software and Espa environment [54,55]. The water bodies added were based on the borderlines of topographic database (NLS) and the water heights were based on the average water heights at the time of scanning. The checked ground points were interpolated by Lagrange's method and visualised. The vertical accuracy of ALS-DTM2 is approximately 0.3 m [53].

4.3. Conventional Nationwide DTMs

Nationwide 25 m × 25 m and 10 m × 10 m grid DTMs (later DTM10 and DTM25) produced by NLS of Finland were used in this study (Figure 4). The elevation values of DTM25 are based on the elevation data and water elements of the topographic database; in other words, on digitised and interpolated contour lines of base maps of the 1990s. The vertical accuracy of DTM25 is 1.76 m referenced to the national reference points of elevation [55,56]. DTM10 has been produced since 2001 along with the update and maintenance of the topographic database. In the aforementioned updating process, water heights and shorelines, heights digitized in stereo workstations, heights of water elements and other known elevation heights are added and data points of contour lines are checked [55,56]. The vertical error of DTM10 is 1.4 m (95% of cases and 2 m 99% of cases) [57].

Figure 4. DTMs used in this study. (**a**) Pairs and groups of DTMs; (**b**) DTMs were processed before analysis with the filling algorithm and the original DTMs were subtracted from the processed DTMs. In this process, the depression pixels and their depths were delineated. The depression pixels were selected and converted to polygons, for which the depression variables were computed based on the processed DTMs.

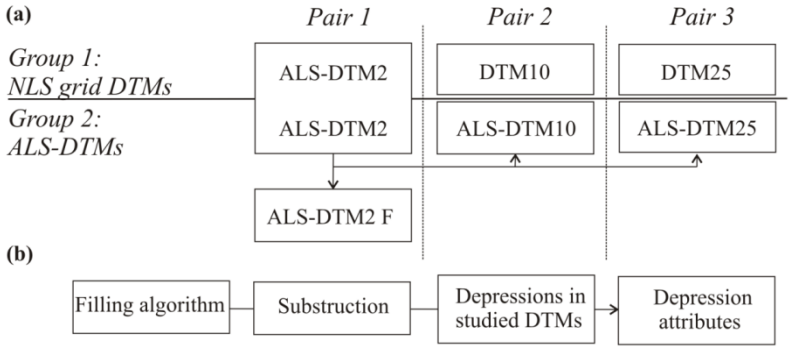

4.4. Input Data Processing

In this study, ALS-DTM2 was resampled to 10 m × 10 m and 25 m × 25 m DTMs (later ALS-DTM10 and ALS-DTM25) by using nearest-neighbour method. This method is commonly applied in studies that concentrate on the impacts of different grid sizes of DTMs on terrain variables [26]. Method delineates new elevation values to output data without changing input elevations in any other way. The changes in elevation values results from the resolution changes made. Thus, it was possible to compare DTMs that represent the same grid size but different acquisition and processing methods. Furthermore, the idea was to find alternatives to the high-resolution DTMs used in studies that require high accuracy with DTMs that are faster to process. In our study, it was stated that the high-resolution DTMs are used instead of DTMs with smaller representative accuracy but the same grid and data sizes because of the growing availability of high-resolution ALS-DTMs. Furthermore, the ALS-DTM2 was

filtered with mean filter (later ALS-DTM2 F) to delineate whether the representation of depressions changed essentially from a flood risk perspective and if the number of small-in-volume depressions and data sizes decreased. Consequently, this study was based on two elevation model groups and three pairs of DTMs (Figure 4). Nevertheless, all DTMs were studied crosswise in statistical methods and some tables and figures summarise all DTMs studied.

DTMs were processed with the depression filling algorithm developed by Wang and Liu [1] (Table 1). This algorithm processes the grid from the edge areas to the inner parts by using the least-cost search technique and raising the original elevation of a pixel (Elevation(n)) to its spill elevation (Spill(c)) when needed. Spill elevation is the smallest elevation value to which the elevation value of processed pixel needs to be raised in order for water to flow from the processed pixel to the actual pour point of a grid. The pixel processing order is based on least-cost search-algorithm, which selects the direction of propagation based on the smallest spill elevation value. Thus, the depression-less flow path follows the spill elevations which become smaller towards the lower reaches. The algorithm was chosen because of its small memory requirements and time complexity for large high-resolution ALS-DTMs. A selection between filling algorithms was not essential because of the parallel results among available filling algorithms, as also mentioned by Dhun [4].

Table 1. Pseudo-code for Wang and Liu algorithm [1].

Line	Code
1	For b ← [cells on data boundary]
2	Spill[b] ← Elevation[b]
3	OPEN.push(Spill[b])
4	While OPEN is not empty
5	c ← OPEN.top()
6	OPEN.pop(c)
7	CLOSED[c] ← true
8	For n ← [neighbours of c]
9	If n ϵ OPEN or CLOSED[n] = true
10	Then [do nothing]
11	Else
12	Spill[n] ← Max(Elevation[n], Spill[c])
13	OPEN.push(n)

Notes: The spill elevation values are delineated starting from the lowest elevation pixel in the border of the elevation data. A priority queue is declared as OPEN and it includes row number, column number and spill elevation variables. The priority queue OPEN includes OPEN.push(), OPEN.top() and OPEN.pop() functions. Function .push adds new nodes to the queue, .top finds the least-cost nodes and .pop removes least-cost nodes from the queue. The array is declared as CLOSED and it marks the pixels that are processed as the central pixels and removed from the OPEN queue.

4.5. Statistical Methods

The variation of depression variables in DTMs was examined both within and between SBAs using descriptive statistics and statistical techniques. Descriptive statistics were mean, median and mode as measures of central tendency, and standard deviation, minimum, maximum and percentiles as

measures of dispersion. The statistical techniques were parametric Levene's test and independent samples *t*-test, and also nonparametric Kolmogorov-Smirnov test, Mann-Whitney U test and Kruskal-Wallis test. The variables considered were mean depth of depression, and its number of pixels, area and volume.

The research between SBAs focused on finding reasons for region dependency of depression variables, while the research within SBAs was based on scale and acquisition method dependency. In this study, parametric and non-parametric statistical techniques were used in parallel, as the fulfilment of the assumptions of the parametric tests varied. In cases in which the aforementioned results differed, the most probable result was considered.

4.6. Error Models

The elevation differences between gathered field reference data and DTMs were discovered by digital elevation models of difference (DoD). These were made by subtracting elevation values of DTMs from the elevation values of reference data points by using corresponding elevation values from DTMs. Minimum, maximum and mean errors, standard deviations and root mean squared errors (RMSEs) were calculated to describe the accuracy of DTMs in representing depressions. We also applied the Nash-Sutcliffe model efficiency coefficient (NSE) to the predictive accuracy of a DTM performance compared with field reference data (Equation (1)):

$$NSE = 1 - \left(\frac{\sum_{i=1}^{n} (Y_{s,i} - Y_{m,i})^2}{\sum_{i=1}^{n} (Y_{s,i} - Y_{mean})^2} \right) \quad (1)$$

where $Y_{s,i}$ is the *i*th surveyed elevation; $Y_{m,i}$ is the *i*th modelled elevation; Y_{mean} is the mean surveyed elevation; and *n* is the total number of observations [58,59]. NSE ranges between $-\infty$ and 1.0, in which NSEs from 0.0 to 1.0 are acceptable levels of performance, NSE 1.0 is the optimum and NSE < 0.0 means unacceptable performance in which the mean value of surveyed data is a better predictor than the simulated values. It has been applied in hydrologic and hydraulic simulations [58,59], but it has also been used to describe the predictive accuracy of other models, like suspended sediment and morphodynamic models [60,61].

After the above-mentioned statistics were established, the depths of depression pixels were compared with the most accurate DTM with error models in which depth errors were examined as matrix of absolute values. The error values were calculated by subtracting depression pixel values of DTMs studied and converting errors to absolute values. The dispersions of these error values, the maximum and mean errors, standard deviations and surface area of error in SBAs were delineated.

4.7. Detention Area Survey

The threshold value for depression volume was delineated to 6000 m^3 based on the example presented in the general plan for flood risk management of the municipality of Ilmajoki (Figure 3) [62]. Preconditions were also set for the location, according to which the depressions located on acceptable land use classes and at a range of 500 m from the stream channel were accepted. The selection between land use classes was based on CORINE Land Cover, in which all but artificial areas were accepted.

This survey was performed on depressions from which the river network was cut off. On the whole, the detention area survey performed exemplified the spatial distribution of the error within SBAs.

5. Results

5.1. Accuracy Assessment of Depressions in DTMs Used

In our study, ALS-DTM2 was the most accurate DTM compared with reference data with RMSEs ranging from 0.176 to 0.406 m (Table 2). R^2 values of fitted linear regression lines of scatter plots representing field reference elevations versus DTM elevations ranged from 0.947 to 0.982 and NSEs ranged from 0.933 to 0.982 (Tables 2 and 3, Figure 5). ALS-DTM2 F was the next most accurate and DTM25 was the least accurate DTM. NSEs of DTM25 are viewed as unacceptable performance [59]. DTM10 and ALS-DTM25 also had large RMSE values (0.728–1.698 m), unacceptable NSE values ((−0.844)–0.48) and R^2 values ranged from 0.100 to 0.670. Only ALS-DTM2, ALS-DTM2 F and ALS-DTM10 had NSEs that were considered as acceptable; in addition, ALS-DTM25 in reference area G had an acceptable performance value of 0.51. The absolute mean errors were also calculated in order to delineate the mean amount of the depth error (Table 2).

Figure 5. Scatter plots of reference data versus DTM elevations in reference area B. (**a**) ALSDTM2; (**b**) ALS-DTM2 F; (**c**) ALS-DTM10; (**d**) DTM10; (**e**) ALS-DTM25; (**f**) DTM25.

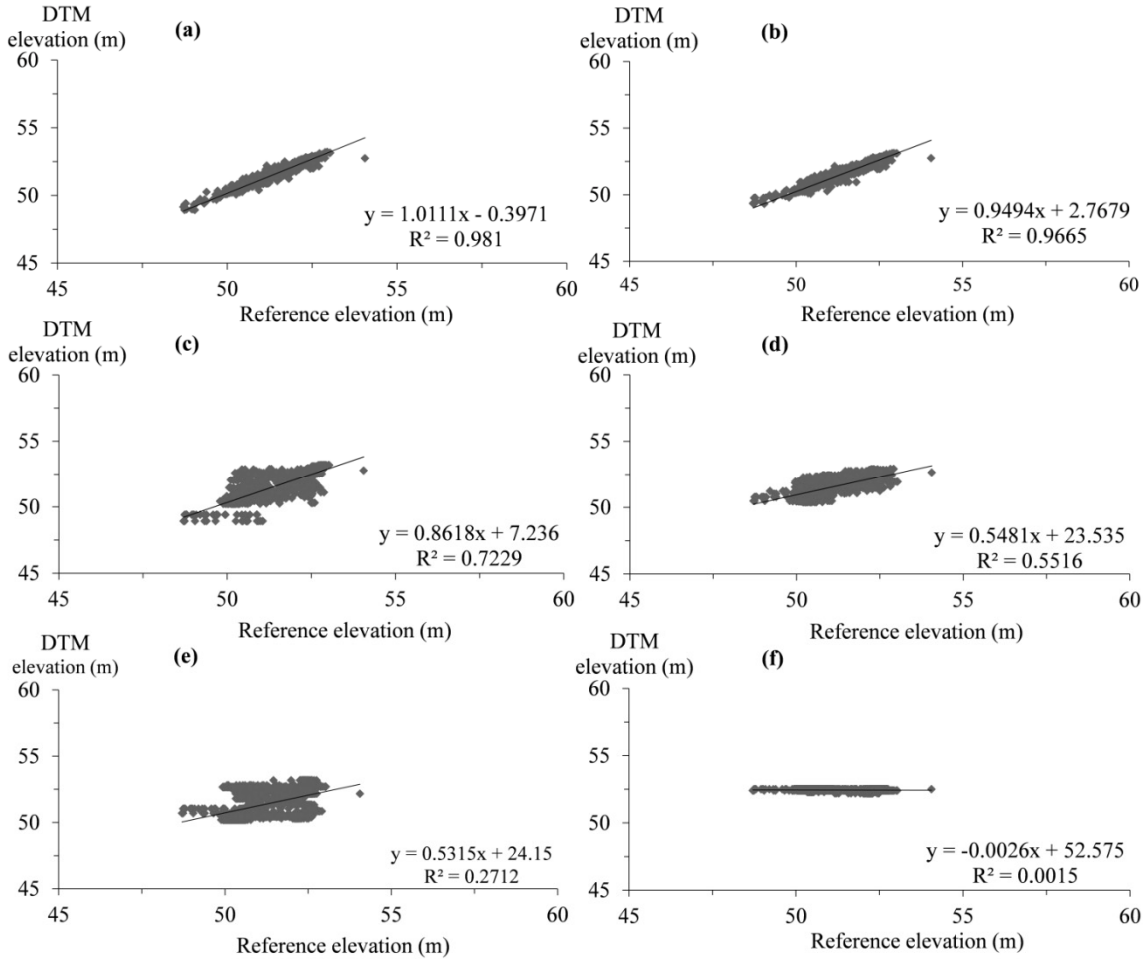

Table 2. Difference between reference data and DTMs. N is the number of reference points in the reference area.

DTM	Area	N	Minimum dz (m)	Maximum dz (m)	Absolute mean error (m)	RMSE (m)	NSE
ALS-DTM2	A	2355	−2.27	4.097	0.230	0.406	0.958
ALS-DTM2 F	A	2355	−2.29	4.279	0.249	0.426	0.951
DTM10	A	2355	−4.32	3.599	0.949	1.183	0.480
ALS-DTM10	A	2355	−3.90	4.029	0.521	0.839	0.816
DTM25	A	2355	−6.62	3.345	2.641	3.318	−0.594
ALS-DTM25	A	2355	−5.69	5.259	0.998	1.601	0.375
ALS-DTM2	B	2836	−1.03	1.132	0.184	0.214	0.949
ALS-DTM2 F	B	2836	−1.01	1.313	0.200	0.243	0.927
DTM10	B	2836	0.00	1.408	0.540	0.728	0.130
ALS-DTM10	B	2836	−2.42	2.309	0.337	0.528	0.684
DTM25	B	2836	−3.76	1.557	1.261	1.538	−0.556
ALS-DTM25	B	2836	−2.74	2.207	0.595	0.918	0.058
ALS-DTM2	C	731	−2.22	1.298	0.238	0.321	0.966
ALS-DTM2 F	C	731	−2.08	1.428	0.265	0.352	0.954
DTM10	C	731	−4.73	2.103	1.040	1.492	−0.574
ALS-DTM10	C	731	−3.37	3.349	0.609	0.899	0.710
DTM25	C	731	−5.41	1.472	1.802	2.493	−0.999
ALS-DTM25	C	731	−5.27	4.175	1.093	1.594	0.202
ALS-DTM2	D	578	−2.77	1.045	0.259	0.391	0.933
ALS-DTM2 F	D	578	−2.51	1.317	0.326	0.464	0.896
DTM10	D	578	−3.13	1.549	1.484	1.698	−0.368
ALS-DTM10	D	578	−3.83	2.697	0.731	1.161	0.459
DTM25	D	578	−3.65	1.895	2.038	2.369	−0.679
ALS-DTM25	D	578	−3.73	3.656	1.196	1.643	−0.202
ALS-DTM2	E	922	−1.81	0.825	0.174	0.324	0.954
ALS-DTM2 F	E	922	−1.73	1.071	0.214	0.357	0.939
DTM10	E	922	−2.89	4.380	1.000	1.290	−0.052
ALS-DTM10	E	922	−3.17	2.533	0.428	0.741	0.749
DTM25	E	922	−3.86	1.935	1.456	1.923	−1.866
ALS-DTM25	E	922	−3.37	4.793	1.224	1.606	−0.844
ALS-DTM2	F	865	−1.57	5.656	0.134	0.294	0.977
ALS-DTM2 F	F	865	−1.56	5.618	0.160	0.323	0.971
DTM10	F	865	−1.92	5.734	1.121	1.368	−0.825
ALS-DTM10	F	865	−3.09	5.678	0.349	0.585	0.906
DTM25	F	865	−5.54	4.867	2.434	3.091	−0.734
ALS-DTM25	F	865	−4.87	5.362	0.810	1.311	0.510
ALS-DTM2	G	1734	−0.98	2.234	0.104	0.176	0.982
ALS-DTM2 F	G	1734	−1.06	2.151	0.123	0.202	0.976
DTM10	G	1734	−3.58	3.776	1.018	1.271	0.203
ALS-DTM10	G	1734	−2.79	2.735	0.307	0.543	0.851
DTM25	G	1734	−5.03	1.519	3.904	4.115	−0.161
ALS-DTM25	G	1734	−4.35	4.078	0.768	1.250	0.305

Table 3. R^2 values of fitted regression lines of scatter plots representing DTM elevations *versus* reference elevations. Scatter plots with fitted linear regression lines were used for the Nash-Sutcliffe model efficiency coefficient (NSE) evaluation, as recommended by [63–65], because of the high extreme values that could affect the NSE because of the squared differences.

DTM/Area	A	B	C	D	E	F	G
ALS-DTM2	0.9633	0.9810	0.9782	0.9468	0.9594	0.9776	0.9824
ALS-DTM2 F	0.9590	0.9665	0.9723	0.9327	0.9503	0.9733	0.9773
DTM10	0.6697	0.5516	0.4137	0.5587	0.3337	0.5929	0.3709
ALS-DTM10	0.8326	0.7229	0.7429	0.5506	0.7755	0.9111	0.8532
DTM25	0.0091	0.0015	0.0030	0.0273	0.0073	0.0005	0.0053
ALS-DTM25	0.4717	0.2712	0.3520	0.1636	0.0995	0.6060	0.3835

5.2. Depression Variables in DTMs Studied

The total area of depressions, total number of depression pixels, area of depressions per km^2 and depression area in relation to the total surface area of SBA decreased with increasing grid size in both DTM groups (Tables 4 and 5). In the group of NLS grid DTMs, the number of depressions was the smallest in DTM10 and the largest in ALS-DTM2. Thus, depressions per km^2 and number of depressions per one pixel of SBA were smallest in DTM10. In the group of ALS-DTMs, the amount of depressions per one pixel of SBA increased owing to resampling process, whereas the number of depressions decreased with increasing grid size.

There were a large number of small depressions in terms of both area and volume in DTMs studied. Depressions were the deepest in DTM25 and ALS-DTM25 (Table 6). Median and mode of depression volume were also the largest in DTM25 in the group of NLS grid DTMs, whereas volume, area and mean depth of depressions were the smallest and the shallowest in ALS-DTM2 (Table 6). Conversely, the measures of the central tendency of the depression area and the pixel number in a depression were largest in DTM10. In the group of ALS-DTMs, the mean depths (medians 0.02–0.12 m), volumes (medians 0.11–91.25 m^3) and areas (medians 4–625 m^2) of depressions increased with grid size.

Single-pixel depressions were predominant in DTMs studied. The relative number of these mainly increased with grid size (46.3%–79.8%), whereas the absolute number of single-pixel depressions mainly decreased in both DTM groups with increasing grid size (Table 4). Yet, single-pixel depressions were small in volume, the ratio of the total volume of single-pixel depressions to the total volume of depressions increased (0.4%–22.3%) mainly with grid size in the group of ALS-DTMs (Appendix 1). In the group of NLS grid DTMs, the DTM10 departed from the aforementioned trends with a relatively small number of single-pixel depressions (10.6%–17.9%) and their volumes (0.002%–0.02%).

Shallow depressions (mean depth ≤0.3 m) were great in number. The absolute number of shallow depression pixels decreased with increasing grid size in both DTM groups (Table 4). Furthermore, the mean depth (medians 0.02–0.10 m) and median volume (0.11–63.12 m^3) of depressions increased with grid size (Appendix 2). In the group of NLS grid DTMs, the absolute number of shallow depressions was smallest in DTM10 (Table 4). Furthermore, the ratio of the number of shallow depressions to the total number of depressions (92.3%–93.9%) and their area to the total depression area (44.1%–57.5%) was smallest in DTM10. These depressions were nevertheless largest in area (medians 750–1500 m^2)

(Appendix 2). The proportion of the total volume (36.7%–89.1%) and the total area (77.6%–97.5%) of shallow depressions to the total depression volume and total area were largest in DTM25, however. In the group of ALS-DTMs, the total surface areas of the shallow depressions decreased with increasing grid size. The volumes (medians 0.11–63.12 m^3), areas (medians 4–625 m^2) and mean depths (medians 0.02–0.08 m) of depressions also followed this negative trend (Table 4, Appendix 2). The total volume of shallow depressions was largest in ALS-DTM10 and smallest in ALS-DTM25 (Table 4). Moreover, the proportion of the number of shallow depressions to the total number of depressions (76.0%–99.9%) and their area to the total area of depressions (46.0%–84.0%) decreased with increasing grid size.

Table 4. Depression variables in Kainastonjoki River study area.

DTM/depression type	Depression n	Depression pixel n	Total depression volume (m^3)	Total depression area (m^2)
ALS-DTM2				
all depressions	575,360	3,609,277	2,603,767	14,437,108
shallow depressions	574,880	3,029,933	854,636	12,119,732
single-pixel depressions	266,391	266,391	24,114	1,065,564
ALS-DTM2 F				
all depressions	199,738	2,874,104	2,262,584	11,496,416
shallow depressions	199,615	2,322,308	611,057	9,289,232
single-pixel depressions	63,903	63,903	2127	255,612
DTM10				
all depressions	311	37,766	1,202,827	3,776,600
shallow depressions	292	16,646	187,623	1,664,600
single-pixel depressions	41	41	61	4,100
ALS-DTM10				
all depressions	46,257	112,383	2,752,926	11,238,300
shallow depressions	39,544	84,463	988,415	8,446,300
single-pixel depressions	32,264	32,264	473,651	2,528,125
DTM25				
all depressions	946	3,127	214,935	1,954,375
shallow depressions	944	3,048	191,498	1,905,000
single-pixel depressions	597	597	37,312	373,125
ALS-DTM25				
all depressions	5,268	12,250	2,263,789	7,656,250
shallow depressions	4,248	8,409	705,231	5,255,625
single-pixel depressions	4,045	4,045	473,651	2,528,125

The number of all depression types, their total volumes and total areas decreased when ALS-DTM2 was filtered (Table 4). The largest filtering effect focused on the number of depressions as the filtered ALS-DTM2 included 30%–35% of the total depression number, 74%–80% of the total depression area and 87%–92% of total depression volume of ALS-DTM2. Furthermore, the area and number of depressions per km^2 and also depressions per one pixel of SBA decreased owing to filtering (Table 5). The mean filter reduced the measures of central tendency of depression mean depth; whereas the effect on depression volume, area and number of pixels forming depressions was mainly the reverse (Table 6). The filtering method reduced the measures of central tendency of the mean depth (medians from 0.02 to 0.01 m) of shallow depressions, whereas the measures of depression area increased (medians from 4 to 12 m^2). The ratio of the total volume of shallow and single-pixel depressions to the total depression volume and the ratio of the total area of shallow and single-pixel depressions to the

total area of depressions decreased owing to filtering (Table 4). Additionally, mean filter decreased the mean depths of single-pixel depressions (medians from 0.01 to 0.004 m), and thus the measures of central tendency of volumes decreased (medians from 0.05 to 0.02 m^3) (Appendix 1).

The number of all depression types, depression number per km^2, depression area per km^2, depression area in relation to the total surface area of SBA and depressions per one pixel of SBA were mainly larger in ALS-DTM10 than in DTM10 (Tables 4 and 5). Depressions were also deeper, in regards to measures of central tendency, in ALS-DTM10 (means 0.14–0.17 m) than in DTM10 (means 0.06–0.11 m), whereas DTM10 represented depressions larger in volume and area than ALS-DTM10 (Table 6). The total area and volume of shallow and single-pixel depressions were mainly larger in ALS-DTM10 than in DTM10 (Table 4). Furthermore, the proportion of the total volume of the single-pixel and shallow depressions to the total volume of all depressions and also the proportion of the total area of aforementioned depressions to the total area of all depressions were mainly larger in ALS-DTM10 (17%–36%; 65%–75%) than in DTM10 (16%–21%; 44%–58%) (Table 4). The shallow depressions in the ALS-DTM10 were smaller in area (medians 100 m^3) and volume (medians 7–9 m^3) than in DTM10 (medians 750–1500 m^2; 30–41 m^3) (Appendix 2). Single-pixel depressions were deeper in ALS-DTM10 (medians 0.05–0.08 m) and larger in volume (medians 5.2–7.8 m^3), than in DTM10 (medians 0.003–0.1 m; 0.3–1 m^3) (Appendix 1).

The ALS-DTM25 included a larger number of all depression types studied than DTM25; in addition, the total number of depression pixels, total volumes and areas of depressions were larger (Table 4). The number and area of depressions per km^2 were also larger in ALS-DTM25 than in DTM25 (Table 5). Also, depression area in relation to the total surface area of SBA (5.8%–13.8%) and the number of depressions per one pixel of the studied watershed (0.03–0.04/km^2) were larger in ALS-DTM25 than in DTM25 (2.3%–8.3%; 0.007–0.02/km^2) (Table 5). The differences between DTM25 and ALS-DTM25 depression variables were small (Table 6). In the ALS-DTM25, the depressions were mainly larger, regarding their mean and median depth (medians 0.1 m) and volume (medians 81–91 m^3), than in DTM25 (0.1 m; 63 m^3) when the standard deviations (SDEs), maximum values of variables and percentiles were taken into account. Furthermore, mean depth, pixel number in a depression, volume and area of shallow depressions were parallel, although the depressions were slightly larger in volume, area and mean depth in DTM25 (Appendix 2). The total volume and area of the single-pixel depressions were larger in ALS-DTM25 than in DTM25 (Appendix 1). Additionally, the relative number of single-pixel depressions to the total area and volume of all depressions were larger in ALS-DTM25 (17%–41%; 8%–22%) than in DTM25 (16%–27%; 7%–17%). The studied depression variables of single-pixel depressions were parallel in DTM25 and ALS-DTM25 when the standard deviations were taken into account.

Table 5. Distribution of depressions in Kainastonjoki River study area.

DTM	Depression area/km^2	Depressions/km^2	% depression area of SBA	Depressions/one pixel of SBA
ALS-DTM2	166,422	6,632	16.6	0.0265
ALS-DTM2 F	132,249	2,298	13.2	0.0092
DTM10	43,534	4	4.4	0.0004
ALS-DTM10	129,548	533	13.0	0.0533
DTM25	22,531	11	2.3	0.0068
ALS-DTM25	88,256	61	8.8	0.0380

Table 6. Statistical variables of all depressions in the Lehmäjoki River SBA; (**a**) ALS-DTM2 and ALS-DTM2 F; (**b**) DTM10 and ALS-DTM10; and (**c**) DTM25 and ALS-DTM25.

	ALS-DTM2				ALS-DTM2 F			
(a)	**Pixels/ depression**	**Mean depth (m)**	**Volume (m^3)**	**Area (m^2)**	**Pixels/ depression**	**Mean depth (m)**	**Volume (m^3)**	**Area (m^2)**
Mean	9.34	0.03	10.75	37.37	23.31	0.02	29.69	93.23
Median	2.00	0.02	0.13	8.00	3.00	0.01	0.13	12.00
Mode	1.000	0.002	0.008	4.000	1.000	0.001	0.004	4.000
SDE	772.02	0.04	2,330.56	3,088.07	1,363.55	0.03	4,071.90	5,454.19
Minimum	1.000	0.001	0.004	4.000	1.000	0.001	0.004	4.000
Maximum	493,837	3.72	1,662,117	1,975,348	497,226	3.72	1,667,566	1,988,904
Percentiles								
25	1.000	0.008	0.040	4.000	1.000	0.005	0.031	4.000
75	4.00	0.04	0.46	16.00	8.00	0.02	0.64	32.00

	DTM10				ALS-DTM10			
(b)	**Pixels/ depression**	**Mean depth (m)**	**Volume (m^3)**	**Area (m^2)**	**Pixels/ depression**	**Mean depth (m)**	**Volume (m^3)**	**Area (m^2)**
Mean	57.49	0.11	2,604.54	5,748.826	3.63	0.14	119.19	363.02
Median	9.00	0.06	45.35	900.00	1.00	0.06	9.20	100.00
Mode	1.000	0.002	0.200	100.000	1.000	0.007	0.700	100.000
SDE	427.14	0.18	34,961.60	42,713.77	85.81	0.20	6,912.35	8,581.18
Minimum	1.000	0.001	0.100	100.000	1.000	0.001	0.100	100.000
Maximum	17,954	3.34	1,684,317	1,795,400	18,676	3.54	1,524,178	1,867,600
Percentiles								
25	2.000	0.002	5.599	200.000	1.000	0.023	2.800	100.000
75	30.00	0.14	359.38	3,000	2.00	0.18	30.80	200.000

	DTM25				ALS-DTM25			
(c)	**Pixels/ depression**	**Mean depth (m)**	**Volume (m^3)**	**Area (m^2)**	**Pixels/ depression**	**Mean depth (m)**	**Volume (m^3)**	**Area (m^2)**
Mean	3.81	0.10	532.96	2,381.27	4.10	0.19	1,082.06	2,561.96
Median	1.00	0.10	62.50	625.00	1.00	0.10	80.63	625.00
Mode	1.000	0.100	62.499	625.000	1.000	0.004	2.500 [a]	625.000
SDE	41.64	0.03	13,499.30	26,024.013	52.94	0.26	23,446.43	33,090.2014
Minimum	1.000	0.100	62.500	625.000	1.000	0.001	0.625	625.000
Maximum	2,729	1.43	671,376	1,705,625	2,992	2.52	1,480,272	1,870,000
Percentiles								
25	1.00	0.10	62.50	625.00	1.00	0.04	25.63	625.00
75	2.25	0.10	187.50	1,406.25	2.00	0.24	248.13	1,250.00

Note: [a] Variable has multiple modes, from which the smallest is represented in the table.

5.3. Statistical Methods

The statistical distributions of depression variables diverged between corresponding DTMs of SBAs. This variation was statistically significant ($p < 0.05$) in the majority of variables (Tables 7 and 8). ,argest similarities were found in volumes of DTM10 and DTM25. Furthermore, the distribution of

depression variables within SBA varied with grid size, acquisition method and processing method of a grid DTM ($p < 0.05$) with some similarities.

Some particular statistical characteristics were found: (1) the distributions of depression variables diverged statistically from ALS-DTM2 within areas. Thus, the statistical variation of depression variables between ALS-DTM2 and ALS-DTM2 F was statistically significant ($p < 0.001$); (2) The statistical distributions of depression variables differed ($p < 0.001$) between DTM10 and ALS-DTM10 within areas; (3) The amount of statistical similarity was greatest between DTM25 and ALS-DTM25.

Table 7. Kruskal-Wallis test results, when the similarities of distributions of the depression variables were studied (**a**) within SBAs (**b**) between SBAs. The confidence level was set to 95%. According to the results the difference of distributions are statistically significant ($p < 0.001$), with some exceptions.

(a)	Kauhajoki River upper reaches	Lehmäjoki River watershed	Nenättömänluoma River watershed
Pixel/depression	$p < 0.001$	$p < 0.001$	$p < 0.001$
Volume of a depression	$p < 0.001$	$p < 0.001$	$p < 0.001$
Area of a depression	$p < 0.001$	$p < 0.001$	$p < 0.001$
Mean depth of a depression	$p < 0.001$	$p < 0.001$	$p < 0.001$

(b)	ALS-DTM2	ALS-DTM2 F	DTM10	ALS-DTM10	DTM25	ALS-DTM25
Pixel/depression	$p < 0.001$	$p < 0.001$	$p < 0.001$	$p < 0.001$	$p < 0.001$	$p < 0.001$
Volume of a depression	$p < 0.001$	$p < 0.001$	$p = 0.104$	$p < 0.001$	$p < 0.001$	$p = 0.082$
Area of a depression	$p < 0.001$	$p < 0.001$	$p < 0.001$	$p < 0.001$	$p < 0.001$	$p < 0.001$
Mean depth of a depression	$p < 0.001$	$p < 0.001$	$p < 0.001$	$p < 0.001$	$p < 0.001$	$p < 0.001$

Table 8. The statistical similarity (X) and difference (*) of the distributions of depression variables (**a**) between SBAs and (**b**) within SBAs, when the Kolmogorov-Smirnov test, Levene's test, independent samples *t*-test and Mann-Whitney U test were used (See notes).

(a)	Trend					
	ALS-DTM2	ALS-DTM2 F	DTM10	DTM25	ALS-DTM10	ALS-DTM25
Lehmäjoki River and Kainastonjoki River SBAs						
Pixels/depression	-/*	-/***	-/***	-/X	-/***	-/***
Volume	*/***	*/***	X/***	X/***	*/***	*/X
Area	***/*	**/***	*/X	X/***	***/***	**/***
Mean depth	***/***	X/***	***/***	X/***	***/***	X/***
Kainastonjoki River and Nenättömänluoma River SBAs						
Pixels/depression	-/***	-/***	-/X	-/X	-/***	-/***
Volume	X/***	X/***	X/X	X/*	X/***	X/X
Area	X/***	X/***	X/X	**/X	X/***	X/***
Mean depth	***/***	X/***	**/*	X/**	***/***	***/**
Lehmäjoki River and Nenättömänluoma River SBAs						
Pixels/depression	-/***	-/***	-/***	-/***	-/***	-/***
Volume	X/***	X/***	X/X	X/***	X/***	*/*
Area	***/***	***/***	**/***	*/***	***/***	***/***
Mean depth	***/***	X/***	X/***	*/***	***/***	***/***

Table 8. *Cont.*

(b)	Trend					
	ALS-DTM2	**ALS-DTM2 F**	**DTM10**	**DTM25**	**ALS-DTM10**	**ALS-DTM25**
Depression volume (upper part) and area (lower part) in Kainastonjoki River						
ALS-DTM2		X/***	**/***	***/***	***/***	***/***
ALS-DTM2 F	***/***		**/***	***/***	***/***	***/***
DTM10	***/***	***/***		**/***	**/***	*/***
DTM25	***/***	***/***	***/***		***/***	***/***
ALS-DTM10	***/***	***/***	***/*	***/***		X/X
ALS-DTM25	***/***	***/***	***/***	***/***	**/***	
Depression mean depth (upper part) and pixels per depression (lower part) in Kainastonjoki River SBA						
ALS-DTM2		***/***	***/***	***/***	***/***	***/***
ALS-DTM2 F	-/***		***/***	***/***	***/***	***/***
DTM10	-/***	-/***		***/***	***/***	***/X
DTM25	-/***	-/***	-/***		***/***	***/***
ALS-DTM10	-/***	-/***	-/***	-/***		***/***
ALS-DTM25	-/***	-/***	-/***	-/***	-/***	
Depression volume (upper part) and area (lower part) in Lehmäjoki River SBA						
ALS-DTM2		*/***	***/***	***/***	**/***	***/***
ALS-DTM2 F	***/***		***/***	**/***	**/***	***/***
DTM10	***/***	***/***		***/***	***/***	*/***
DTM25	***/***	***/***	***/***		*/***	***/***
ALS-DTM10	***/***	***/***	***/***	***/***		X/***
ALS-DTM25	***/***	***/***	***/X	***/***	X/***	
Depression mean depth (upper part) and pixels per depression (lower part) in Lehmäjoki River SBA						
ALS-DTM2		***/***	***/***	***/***	***/***	***/***
ALS-DTM2 F	-/***		***/***	***/***	***/***	***/***
DTM10	-/***	-/***		***/***	**/***	***/***
DTM25	-/***	-/***	-/***		***/***	***/***
ALS-DTM10	-/***	-/***	-/***	-/***		***/*
ALS-DTM25	-/***	-/***	-/***	-/***	-/***	
Depression volume (upper part) and area (lower part) in Nenättömänluoma River SBA						
ALS-DTM2		*/***	**/***	***/***	***/***	***/***
ALS-DTM2 F	***/***		**/***	***/***	***/***	***/***
DTM10	***/***	***/***		**/***	**/***	**/X
DTM25	***/***	***/***	***/***		X/***	***/***
ALS-DTM10	***/***	***/***	***/***	***/***		**/X
ALS-DTM25	***/***	***/***	***/***	***/***	X/***	
Depression mean depth (upper part) and pixels per depression (lower part) in Nenättömänluoma River SBA						
ALS-DTM2		***/***	***/***	***/***	***/***	***/***
ALS-DTM2 F	-/***		***/***	***/***	***/***	***/***
DTM10	-/***	-/***		***/***	X/***	***/***
DTM25	-/***	-/***	-/***		***/***	***/***
ALS-DTM10	-/***	-/***	-/***	-/***		***/***
ALS-DTM25	-/***	-/***	-/***	-/X	-/***	

Notes: The pairs of DTMs represented by green backgrounds fulfilled the hypothesis of same variances; otherwise, pairs with a red background did not fulfil this hypothesis with 95% confidence value. Red fonts represent pairs that obeyed normal distribution after logarithmic transformation, although non-normal distributions can be dismissed based on central limit theorem in cases where the hypotheses of same variances were fulfilled. Thus, boxes with a red background are read from the right side of the backslash (non-parametric tests) and boxes with a green background are read from the left side (parametric tests). Pixels per depression represent the ordinal scale, and thus only the non-parametric tests were applied. Here *** represents statistically highly significant difference ($p < 0.001$); ** significant difference ($p < 0.01$); and * almost significant difference ($p \leq 0.05$).

5.4. Error Models

A substantial amount of depth error was small in relation to ALS-DTM2 as reference data and also in relation to the vertical errors of the DTMs studied. Thus, the maximum values of errors represented the largest differences between DTMs (Table 9, Figure 6). ALS-DTM10 and ALS-DTM25 had a smaller maximum of errors than DTM10 and DTM25, whereas the filtered ALS-DTM2 had the smallest maximum error values. The maximum errors of ALS-DTMs increased with grid size.

The surface area of studied SBA containing depth error improved the idea about the characteristics of depth error in DTMs (Table 9). The relative proportions of the error surface area increased with grid size in both DTM groups. The filtered ALS-DTM2 included the smallest error surface area (14%–21%). ALS-DTM10 contained a smaller proportion of error area (36%–56%) than DTM10 (48%–63%), whereas the surface areas of error were parallel in DTM25 and ALS-DTM25.

Table 9. Depth error in relation to ALS-DTM2.

Area/DTM	Maximum (m)	Mean (m)	SD (m)	Median (m)	Surface areas of error in SBAs (%)
Kainastonjoki					
ALS-DTM2 F	2.07	0.007	0.03	0.023	19.1
DTM10	6.43	0.03	0.18	0.007	63.1
ALS-DTM10	2.69	0.03	0.09	0.002	35.9
DTM25	6.32	0.03	0.18	0.006	84.3
ALS-DTM25	3.33	0.03	0.10	0.007	84.4
Nenättömänluoma					
ALS-DTM2 F	2.05	0.005	0.04	0.019	13.5
DTM10	8.14	0.06	0.33	0.006	48.2
ALS-DTM10	3.89	0.02	0.11	0.006	47.1
DTM25	8.10	0.04	0.28	0.004	66.7
ALS-DTM25	5.44	0.04	0.19	0.005	66.8
Lehmäjoki					
ALS-DTM2 F	1.54	0.01	0.04	0.025	21.1
DTM10	5.03	0.07	0.22	0.011	59.1
ALS-DTM10	3.52	0.04	0.12	0.008	56.2
DTM25	5.44	0.06	0.24	0.008	77.7
ALS-DTM25	3.71	0.03	0.10	0.008	76.9

Figure 6. The distributions of depth error in (**a**) Kainastonjoki and (**b**) Nenättömänluoma River SBAs. In ALS-DTMs, the surge of depth error occurred at higher percentage points than in NLS grid DTMs.

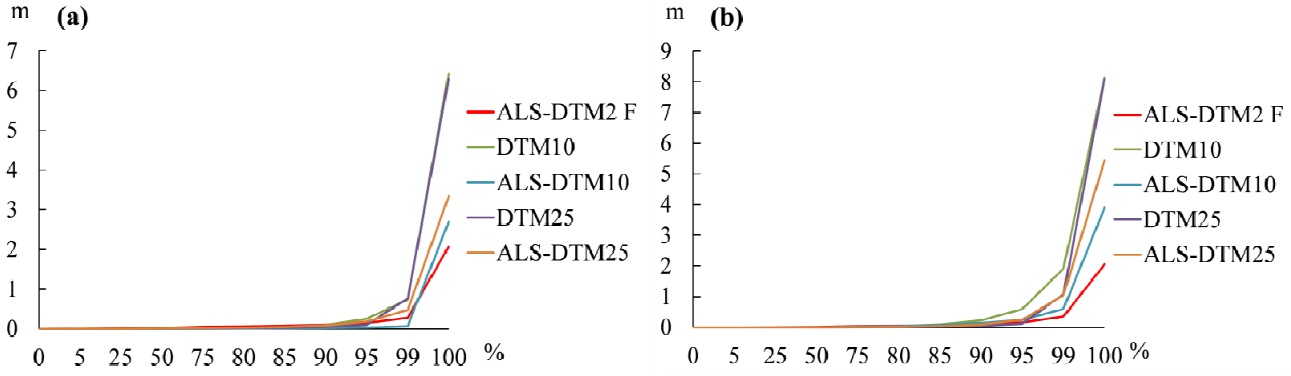

On the whole, the amount of depth error varied uniquely with depression. Figure 7 represents typical characteristics of specific DTMs to describe depressions and also illustrates the formation of depth error.

Figure 7. Terrain and depression representations of DTMs studied. An aerial photograph acts as a background. The blue line illustrates the stream channel and red depressions; when the tone gets darker the depression pixels are deeper.

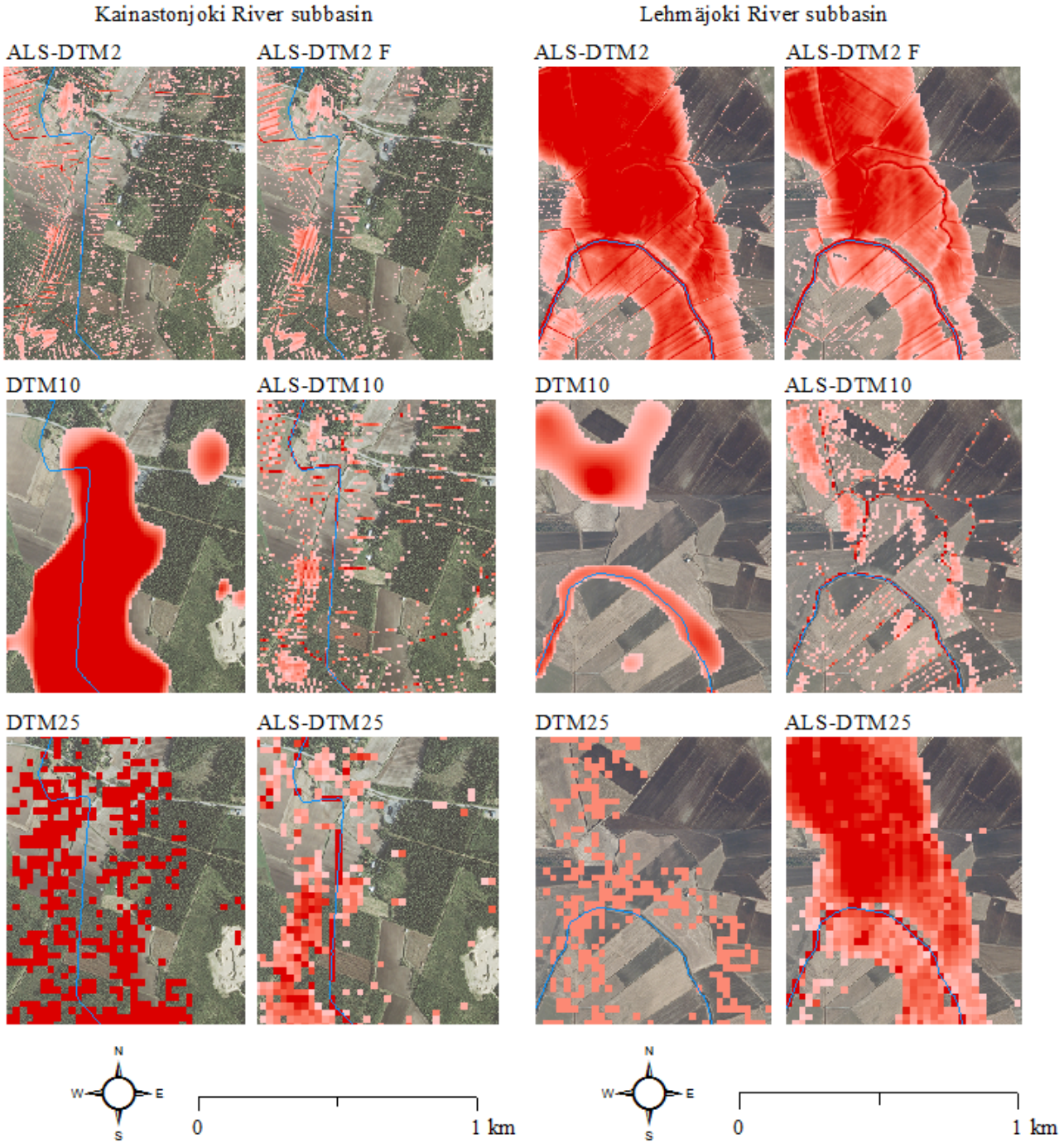

5.5. Survey of Detention Areas for Water

There were differences between locations, total numbers and total volumes of depressions that met the criteria set in Section 4.7 (Figures 8 and 9). The total number of depressions ranged from 7 to 46 and total volume ranged from 1.39 to 3.97 million m^3 between DTMs studied. When the above-mentioned depression variables were compared with the depressions represented in ALS-DTM2, both the DTM25 and ALS-DTM10 varied most from the reference data (Figures 8 and 9). Furthermore, the difference in ALS-DTM2 F, DTM10 and ALS-DTM25 was the smallest.

When the DTMs were studied in more detail some observations were possible: (1) the difference between filtered ALS-DTM and ALS-DTM2 was the smallest with 84% equivalence in total depression number and 96% in total volumes. Filtered ALS-DTM2 was the only DTM that represented all of the largest depressions represented in reference DTM; (2) The difference of depression variables in relation to reference DTM was larger in ALS-DTM10 than in DTM10. ALS-DTM10 represented only 39% of the total depression number and 50% of the total depression volume in relation to the depressions in DTM10; (3) DTM25 differed more from the reference DTM than ALS-DTM25. DTM25 represented 27% of the total depression number and 38% of the total depression volume in relation to the depressions in ALS-DTM25; (4) ALS-DTM25 generalised the terrain representation of ALS-DTM2 as expected, although the ALS-DTM10 was an intermediate form that was lacking some of the information represented in ALS-DTM25.

Figure 8. The modelled detention areas for water: (**a**) number ;and (**b**) volumes of depressions that met the set criteria; (**c**) maximum and (**d**) minimum volumes of depressions chosen.

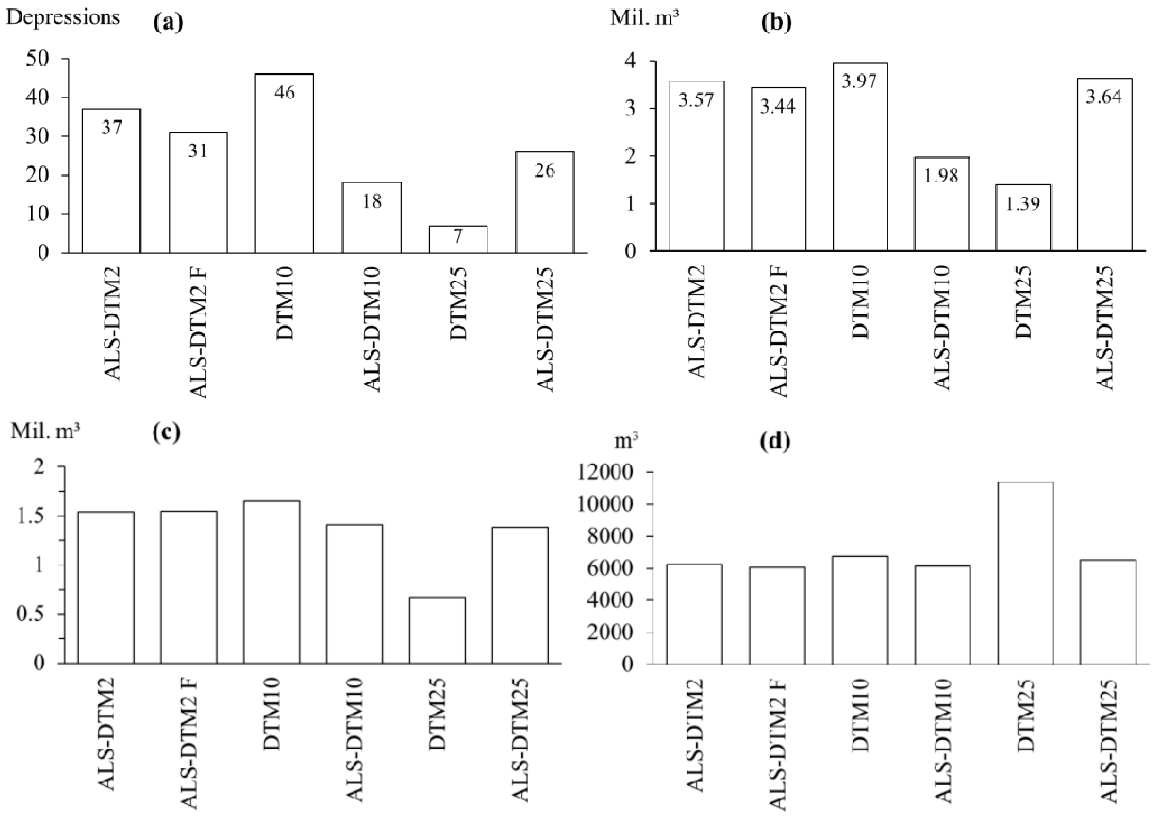

Figure 9. Locations and volume classes of depressions that met the set criteria.

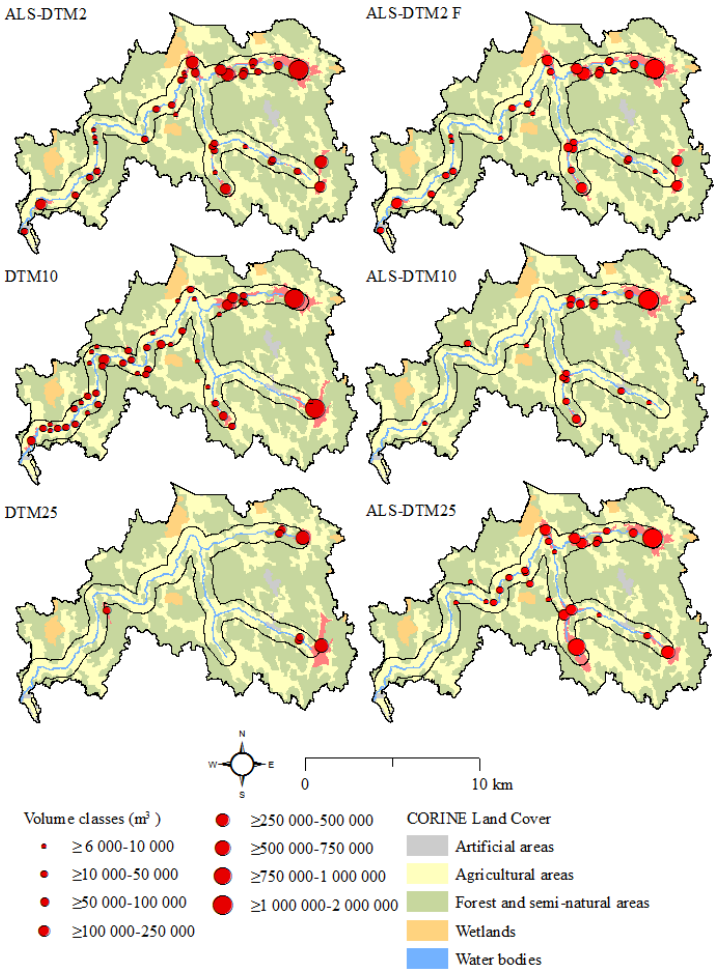

6. Discussion

6.1. The Accuracy of DTMs for Representing Terrain

In our study, ALS-DTM2 was the most accurate DTM used in relation to reference data and also was most successful in terms of terrain representation. ALS-DTMs represented terrain more accurately than nationwide NLS grid DTMs, and also the accuracy of a DTM to represent terrain decreased with increasing grid size in both DTM groups studied. This finding is supported by earlier studies [3,55,66] which assert that the nationwide 25 m × 25 m and 10 m × 10 m NLS grid DTMs do not meet all the modern requirements for representation accuracy. These findings are supported by Oksanen [20] according to whom an increase in the DTM vertical error will increase the error in surface derivatives such as slope, aspect and watershed delineation in fine toposcale elevation datasets that are typically represented in a 5–50 m grid and derived from contour data.

6.2. The Variation of the Hydrological Depression Variables

In our study, acquisition method, processing method and grid size of DTMs affected both the location and the hydrological variables of depressions. Furthermore, the variables studied were dependent on the scale and acquisition method of the DTM and also the area studied. This finding is

supported by Chu *et al*. and colleagues [13,25–27] concerning the area and scale dependency of depression variables. In our study, the depression variables also showed more regularity in the group of ALS-DTMs in which DTMs based on the same acquisition method were resampled than in the group of NLS grid DTMs based on different acquisition and processing methods. Similar results can be also found in earlier studies [10,18].

The number of all depressions and depression pixels decreased with increasing grid size in the group of ALS-DTMs. For example, Abedini *et al*. and colleagues [25–27,33] obtained parallel results in relation to the depression number. In our study, both the shallow and the single-pixel depressions also followed this negative trend in the group of ALS-DTMs. Furthermore, the number of depression pixels followed the aforementioned negative trend in the group of NLS grid DTMs. These observed regularities can mainly be explained by the accurate representation of terrain microtopography in the high-resolution DTMs and the generalisation of this representation with growing grid size [1,26]. In addition, the number of pixels for a given area decreases by a power of two with increasing grid size [31] and consequently explains our findings.

The total areas of depressions followed a decreasing trend with increasing grid size in both DTM groups. This finding can be explained by the changes of both small-in-size and artificial depressions with increasing grid size [26]. The occurrence of small depressions is substantial in high-resolution DTMs. The absolute numbers of small depressions decreases with increasing grid size, because larger grid sizes do not enable the representation of small depressions in the same way as DTMs with smaller grid sizes. Additionally, the vertical accuracy of high-resolution DTM approaches the height difference between neighbouring pixels, resulting in small depressions. This hypothesis needs to be separated from the observation made in our study that DTM25 and ALS-DTM25 included the highest relative numbers of single-pixel depressions. These findings can be partly explained by the squaring of the pixel number with increasing grid size [31] and the fact that the grid size of a DTM affects the accuracy of its terrain representation [26]. Thus, the results of our study parallel those of Zandbergen [26], but diverge from those of Abedini *et al*. [25] and partly diverge from those of Chu *et al*. [13] and also Yang and Chu [27]. According to Abedini *et al*. [25], the total areas of depressions (%) follow an increasing trend with grid size in a group of laser scanning based DTMs. According to Yang and Chu [27], the total areas of depressions followed decreasing trend with grid size in laser scanning based laboratory and field plot surfaces. Whereas, resampled 30 m USGS-DEM followed increasing trend with grid size. According to Chu *et al*. [13], depression area (m^2) is area-dependent. In our study, total areas of depressions varied between SBAs maintaining the trends aforementioned.

In our study, the regional dependency of the depression total volumes was highlighted. This variable did not follow any clear trend between SBAs. Our results are parallel with that of Chu *et al*. [13], in that the regional dependency is influenced by the microtopography of the SBA and also the acquisition method and grid size of the DTM. The results of our study were different from those of earlier studies [25–28,67]. Only the volumes of nationwide NLS grid DTMs in Kainastonjoki and Nenättömänluoma River SBAs followed the decreasing trend with increasing grid size presented by earlier studies [26,28–30]. The generalisation of the terrain representation with increasing grid size is mentioned as the main reason for this negative trend. Kamphorst [67] represents that the total volume of depressions increases at first but is stabilised with increasing grid size.

The mean filter did not change the representation of depressions or the values of depression variables excessively, because in the flood risk management perspective, depressions which are small in volume and separate are not the most essential. Furthermore, the data sizes decreased. Our finding was expected, because the mean filter determines new elevation values based on the neighbouring pixels of processed pixels. The mean filter generalised slightly the elevation values of DTMs. Thus, different kinds of filters are used for reducing data noise and removing small depressions [41,43,68].

ALS-DTM10 and ALS-DTM25 were more accurate in relation to the reference data than DTM10 and DTM25. This difference between NLS grid 10 and ALS-DTM10 is also mentioned by Vilhomaa [55]. In our study, ALS-DTMs included a larger number of all studied depression types than DTM10 and DTM25. Additionally, ALS-DTM10 and ALS-DTM25 included more depressions per square kilometre and per one pixel of SBA. The depression area per square kilometre, relative amounts of depressions from the total area of SBA and relative amounts of single-pixel depressions from all depressions were generally also greater in ALS-DTMs than in DTM10 and DTM25. These results were expected, because ALS-DTM2 represented the terrain microtopography accurately and the generalisation of this due to the resampling process created separate but scattered depression pixels. The difference between ALS-DTM25 and NLS grid DTM25 was the smallest and the difference between ALS-DTM10 and DTM10 was the largest of all pairs studied. The number of depressions was lowest in DTM10, but these depressions were largest in area.

6.3. Error Models and Detention Area Survey

The maximum depth errors in relation to ALS-DTM2 gave us a general idea about the differences between DTMs in terms of representing depressions. Furthermore, error models and statistical parameters illustrated some typical characteristics of specific DTMs for representing certain types of depressions. The spatial distribution of errors and the impact of the depth errors on separate depressions were not seen, however, until more detailed visual examinations were performed.

The results of the detention area survey supported the conclusions drawn from depth error models and statistics, according to which the variables of depressions were acquisition method, processing method and scale dependent. The varying accuracy of specific DTMs in terms of representing separate depressions in relation to reference data was emphasised. This heterogeneous quality of nationwide NLS grid DTMs is also mentioned by earlier studies [22,55]. It is caused by errors in photogrammetric stereo interpretation which are in turn caused by systematic errors in contour data, the low accuracy of terrain elevations, and coverage of terrain that causes difficulties in the interpretation of stereo images. Problems can also arise with the aerial photography techniques available, large grid sizes, different methods used to produce contour lines, problems updating contour lines and the algorithms used to create the elevation datasets. The representation of low-lying and flat areas can be very erroneous because of the generalised terrain representation [69]. In our study, the variation in accuracy was limited by the statistical distribution of depression variables and the results of error models performed. This distribution of error is best described by robust descriptors of distributions as quantiles and maximums, in addition to conventional measures of distribution. This is also supported by Oksanen and Sarjakoski [22].

The results of the detention area survey were the same as those of depth error models in that mean-filtered ALS-DTM2 was the closest to ALS-DTM2. The impact of filtering was particularly evident in the depressions whose volume was near the threshold set. In contrast to error models, DTM10 was closer to ALS-DTM2 than ALS-DTM10 in the detention area survey, whereas ALS-DTM25 was closer to ALS-DTM2 than DTM25, as also shown in error models. The typical ability of DTM10 to represent depressions as unbroken in shape and large in area in relation to other DTMs explains the above-mentioned observations, whereas DTM25 represented the same as a group of scattered pixels. Furthermore, the generalisation of ALS-DTM2 represented depressions with varying degrees of success, depending on the depression examined.

7. Conclusions

Our study has demonstrated the effects of acquisition method, processing method and grid size of nationwide DTMs on the detection of topographic depressions and their hydrological variables. This was performed by using quantitative statistics, digital elevation models of difference and error models. According to our study, the decision about the suitability of the available DTMs for a specific purpose should be made based on the demands of the problem settings and accuracy. In future studies with a relatively low demand for accuracy, awareness of the error, its level, and effects on analyses in general is sufficient. In more accurate studies, the awareness of the varying spatial accuracy of a DTM in representing terrain is emphasised. Furthermore, knowledge about certain typical characteristics of available DTMs in representing a studied terrain variable or variables is essential. Field work also needs to be considered. It is also recommended to use the most accurate DTM that computing resources can process. Furthermore, the interpretation of results is recommended together with the classification of variables under study (e.g., depth classification of depressions), as well as setting thresholds for it (e.g., volumes of depressions considered).

Furthermore, the following specific conclusions can be drawn:

- ALS-DTMs are closer to the real topography of depressions than DTMs based on more conventional acquisition and processing methods. The accuracy of terrain representation decreased with increasing grid size in both groups of DTMs.
- The acquisition method, processing method and grid size of a DTM has an impact on modelled depression variables. This variation was found to be area, acquisition method, processing method and scale dependent.
    - The difference between ALS-DTM10 and DTM10 is the largest. The principal reason was the scattered depression pixels that were great in number because of the resampling process performed. The number of these separate fragmental pixels decreased as the degree of terrain representation became greater with increasing grid size. DTM10 also differed from the other DTMs in terms of statistical significance.
    - The absolute number of depressions and depression pixels is larger in ALS-DTM10 and ALS-DTM25 than in DTM10 and DTM25. This is a consequence of the resampling process of ALS-DTM2 that produces scattered depression pixels.
    - The mean filtering of ALS-DTM2 focuses on the small and shallow depressions, and is thus suitable for detection of water detention areas in flood risk management.

- The maximum pixel depth error of a DTM illustrated the amount of depth error in relation to ALS-DTM2 in a most descriptive way. ALS-DTMs have smaller maximum error values than the nationwide NLS grid DTMs 10 m × 10 m and 25 m × 25 m.
- The accuracy of DTMs in representing separate depressions varied. Thus, the decreasing grid size of a DTM is no guarantee of increasing spatial accuracy when there is a demand for the most accurate data available. According to the aforementioned findings, the acquisition method, processing method and grid size of a DTM have an impact on the location, number and total volumes of depression areas.

Acknowledgments

Funding for this study (GIFLOOD, FLOODAWARE, LuhaGeoIT and RivCHANGE projects) was supplied by the Finnish Funding Agency for Technology and Innovation (Tekes), the Maj and Tor Nessling Foundation, the Ministry of Agriculture and Forestry and the Academy of Finland.

Conflicts of Interest

The authors declare no conflict of interest.

Appendix

Appendix 1. Variables for single-pixel depressions. The mean values are represented in brackets because of the skewed distributions of depression variables.

Area/DTM	Depression number	Median mean depth (m)	SD mean depth (m)	Median volume (m^3)	SD volume (m^3)	Max depth (m)
Upper reaches of Kainastonjoki River SBA						
ALS-DTM2	266,391	0.01 (0.02)	0.03	0.05 (0.09)	0.12	0.51
ALS-DTM2 F	63,903	0.005 (0.008)	0.01	0.02 (0.03)	0.04	0.19
DTM10	41	0.003 (0.01)	0.05	0.30 (1.49)	5.29	0.34
DTM25	597	0.10 (0.10)	0.000002	62.50 (62.50)	0.001	0.10
ALS-DTM10	32,264	0.08 (0.15)	0.19	7.80 (14.98)	18.91	2.74
ALS-DTM25	4045	0.10 (0.19)	0.25	64.38 (117.10)	156.08	4.51
Nenättömänluoma River SBA						
ALS-DTM2	266,830	0.01 (0.02)	0.03	0.04 (0.03)	0.12	0.47
ALS-DTM2 F	55,901	0.005 (0.009)	0.01	0.02 (0.01)	0.04	0.19
DTM10	50	0.004 (0.01)	0.02	0.40 (0.98)	2.25	0.15
DTM25	954	0.10 (0.10)	0.01	62.50 (62.83)	6.71	0.40
ALS-DTM10	29,459	0.07 (0.17)	0.22	7.50 (16.52)	22.12	2.43
ALS-DTM25	3619	0.11 (0.22)	0.30	68.75 (137.19)	186.96	3.72
Lehmäjoki River SBA						
ALS-DTM2	365,225	0.01 (0.02)	0.03	0.04 (0.54)	0.12	0.54
ALS-DTM2 F	76,014	0.004 (0.008)	0.01	0.02 (0.15)	0.04	0.15
DTM10	701	0.01 (0.02)	0.04	1.00 (2.29)	3.90	0.55
DTM25	3178	0.10 (0.10)	0.01	62.50 (62.18)	7.68	0.60
ALS-DTM10	40,073	0.05 (0.14)	0.21	5.20 (13.98)	21.05	2.37
ALS-DTM25	5854	0.08 (0.19)	0.26	52.50 (116.97)	160.63	2.42

Appendix 2. Variables for shallow (mean depth ≤ 0.3 m) depressions. The mean values are represented in brackets because of the skewed distributions of depression variables.

Area/DTM	Depression number	Depression pixel number	Median mean depth (m)	SD mean depth (m)	Median volume (m^3)	SD volume (m^3)	Median area (m^2)	SD area (m^2)
Upper reaches of Kainastonjoki River SBA								
ALS-DTM2	574,880	3,029,933	0.02 (0.03)	0.04	0.14 (1.49)	40.46	8.00 (21.08)	309.68
ALS-DTM2F	199,615	2,322,308	0.01 (0.02)	0.02	0.12 (3.06)	81.94	12.00 (46.54)	397.37
DTM10	292	16,646	0.03 (0.05)	0.06	29.50 (642.55)	2,357.16	1350 (5,700.68)	13,931.44
DTM25	944	3048	0.10 (0.10)	0.006	62.50 (202.86)	496.20	625 (2018)	4,869.32
ALS-DTM10	39,544	84,463	0.07 (0.09)	0.08	9.20 (25)	235.30	100 (213.59)	994.02
ALS-DTM25	4248	8409	0.08 (0.10)	0.08	63.12 (166.01)	1,179.68	625 (1,237.20)	5,150.54
Nenättömänluoma River SBA								
ALS-DTM2	514,387	2,260,555	0.02 (0.03)	0.03	0.11 (1.08)	34.20	4.00 (17.58)	162.14
ALS-DTM2F	156,593	1,573,508	0.01 (0.02)	0.02	0.10 (2.34)	45.92	12.00 (40.19)	260.31
DTM10	434	31,456	0.03 (0.06)	0.07	40.80 (1,124.32)	4,052.12	1500 (7,247.93)	18,371.54
DTM25	1462	3077	0.10 (0.10)	0.004	62.50 (1,315.41)	234.39	625 (1,315.4)	2,253.94
ALS-DTM10	31,026	55,190	0.06 (0.08)	0.08	7.00 (18.33)	147.74	100 (177.88)	715.02
ALS-DTM25	3445	5278	0.08 (0.10)	0.08	55.63 (111.19)	383.61	625 (957.55)	1,784.74
Lehmäjoki River SBA								
ALS-DTM2	777,433	4,916,916	0.02 (0.03)	0.03	0.13 (1.89)	88.50	8.00 (25.30)	487.48
ALS-DTM2F	249,806	3,683,152	0.01 (0.02)	0.02	0.13 (4.12)	112.42	12.00 (58.98)	605.74
DTM10	3630	108,636	0.05 (0.07)	0.07	33.20 (479.81)	2,922.84	750 (2,992.73)	112.90
DTM25	5293	15,686	0.10 (0.10)	0.008	62.50 (195.81)	838.97	625 (1,852.20)	4,851.34
ALS-DTM10	50,649	139,039	0.05 (0.08)	0.07	6.60 (29.97)	475.64	100 (274.51)	1,885.08
ALS-DTM25	6531	15,470	0.07 (0.09)	0.08	53.13 (185.38)	1,012.33	625 (1,480.44)	4,040.79

References

1. Wang, L.; Liu, H. An efficient method for identifying and filling surface depressions in digital elevation models for hydrologic analysis and modelling. *Int. J. Geogr. Inf. Sci.* **2006**, *20*, 193–213.
2. Liu, H.; Wang, L. Mapping detention basins and deriving their spatial attributes from airborne LiDAR data for hydrological applications. *Hydrol. Process.* **2008**, *22*, 2358–2369.
3. Alho, P.; Hyyppä, H.; Hyyppä, J. Consequence of DTM precision for flood hazard mapping: A case study in SW Finland. *Nord. J. Surv. Real Estate Res.* **2009**, *6*, 21–39.
4. Dhun, K. *Application of LiDAR DEMs to the Modelling of Surface Drainage Patterns in Human Modified Landscapes*; The University of Guelph: Guelph, ON, Canada, 2011.

5. Wang, L.; Yu, J. Modelling detention basins measured from high-resolution light detection and ranging data. *Hydrol. Process.* **2012**, *26*, 2973–2984.
6. Hilldale, R.C.; Raff, D. Assessing the ability of airborne LiDAR to map river bathymetry. *Earth Surf. Processes* **2008**, *33*, 773–783.
7. Alho, P.; Kukko, A.; Hyyppä, H.; Kaartinen, H.; Hyyppä, J.; Jaakkola, A. Application of boat-based laser scanning for river survey. *Earth Surf. Processes* **2009**, *34*, 1831–1838.
8. Vaaja, M.; Hyyppä, J.; Kukko, A.; Kaartinen, H.; Hyyppä, H.; Alho, P. Mapping topography changes and elevation accuracies using a mobile laser scanner. *Remote Sens.* **2011**, *3*, 587–600.
9. Bolstad, P.V.; Stowe, T. An evaluation of DEM accuracy—Elevation, slope, and aspect. *Photogramm. Eng. Remote Sens.* **1994**, *60*, 1327–1332.
10. Thompson, J.A.; Bell, J.C.; Butler, C.A. Digital elevation model resolution: Effects on terrain attribute calculation and quantitative soil-landscape modeling. *Geoderma* **2001**, *100*, 67–89.
11. Burdziej, J.; Kunz, M. Effect of digital terrain model resolution on topographic parameters calculation and spatial distribution of errors. In Proceedings of the 26th Annual Symposium of the European Association of Remote Sensing Laboratories (EARSel), Warsaw, Poland, 29 May–2 June 2006; pp. 615–626.
12. Vaze, J.; Teng, J.; Spencer, G. Impact of DEM accuracy and resolution on topographic indices. *Environ. Modell. Softw.* **2010**, *25*, 1086–1098.
13. Chu, X.; Zhang, J.; Yang, J.; Chi, Y. Quantitative evaluation of the relationship between grid spacing of DEMs and surface depression storage. In Proceedings of the World Environmental and Water Resources Congress 2010: Challenges of Change, Providence, RI, USA, 16–20 May 2010; pp. 4447–4457.
14. Haile, A.T.; Rientjes, T. Effects of LiDAR DEM resolution in flood modelling: A model sensitivity study for the city of Tegucigalpa, Honduras. In Proceedings of the ISPRS WG III/3, III/4, V/3 Workshop "Laser scanning 2005", Enschede, The Netherlands, 12–14 September 2005.
15. Wolock, D.M.; Price, C.V. Effects of digital elevation model map scale and data resolution on a topography-based watershed model. *Water Resour. Res.* **1994**, *30*, 3041–3052.
16. Zhang, W.H.; Montgomery, D.R. Digital elevation model grid size, landscape representation, and hydrologic simulations. *Water Resour. Res.* **1994**, *30*, 1019–1028.
17. Gyasi-Agyei, Y.; Willgoose, G.; Detroch, F.P. Effects of vertical resolution and map scale of digital elevation models on geomorphological parameters used in hydrology. *Hydrol. Process.* **1995**, *9*, 363–382.
18. Li, J.; Wong, D.W.S. Effects of DEM sources on hydrologic applications. *Comput. Environ. Urban* **2010**, *34*, 251–261.
19. Wu, S.; Li, J.; Huang, G.H. Characterization and evaluation of elevation data uncertainty in water resources modeling with gis. *Water Resour. Manag.* **2008**, *22*, 959–972.
20. Oksanen, J. *Digital Elevation Model Error in Terrain Analysis*; Academic Dissertation in Geography, University of Helsinki: Helsinki, Finland, 2006.
21. Oksanen, J. Tracing the gross errors of DEM—Visualisation techniques for preliminary quality analysis. In Proceedings of the 21st International Cartographic Conference, Durban, South Africa, 10–16 August 2003.

22. Oksanen, J.; Sarjakoski, T. Uncovering the statistical and spatial characteristics of fine toposcale DEM error. *Int. J. Geogr. Inf. Sci.* **2006**, *20*, 345–369.
23. Oksanen, J.; Sarjakoski, T. Error propagation analysis of DEM-based drainage basin delineation. *Int. J. Remote Sens.* **2005**, *26*, 3085–3102.
24. Oksanen, J.; Sarjakoski, T. Error propagation of DEM-based surface derivatives. *Comput. Geosci.* **2005**, *31*, 1015–1027.
25. Abedini, M.J.; Dickinson, W.T.; Rudra, R.P. On depressional storages: The effect of DEM spatial resolution. *J. Hydrol.* **2006**, *318*, 138–150.
26. Zandbergen, P.A. The effect of cell resolution on depressions in digital elevation models. *Appl. GIS* **2006**, *2*, doi:10.2104/ag060004.
27. Yang, J.; Chu, X. Effects of DEM resolution on surface depression properties and hydrologic connectivity. *J. Hydrol. Eng.* **2013**, *18*, 1157–1169.
28. Huang, C.; Bradford, J.M. Depressional storage for markov-gaussian surfaces. *Water Resour. Res.* **1990**, *26*, 2235–2242.
29. Carvajal, F.; Aguilar, M.A.; Aguera, F.; Aguilar, F.J.; Giraldez, J.V. Maximum depression storage and surface drainage network in uneven agricultural landforms. *Biosyst. Eng.* **2006**, *95*, 281–293.
30. Alvarez-Mozos, J.; Angel Campo, M.; Gimenez, R.; Casali, J.; Leibar, U. Implications of scale, slope, tillage operation and direction in the estimation of surface depression storage. *Soil Tillage Res.* **2011**, *111*, 142–153.
31. Lindsay, J.B.; Creed, I.F. Sensitivity of digital landscapes to artifact depressions in remotely-sensed DEMs. *Photogramm. Eng. Remote Sens.* **2005**, *71*, 1029–1036.
32. Zandbergen, P.A. Accuracy considerations in the analysis of depressions in medium-resolution LiDAR DEMs. *Gisci. Remote Sens.* **2010**, *47*, 187–207.
33. Ullah, W.; Dickinson, W.T. Quantitative description of depression storage using a digital surface model. 2. Characteristics of surface depressions. *J. Hydrol.* **1979**, *42*, 77–90.
34. Chi, Y.; Yang, J.; Chu, X. Characterization of surface roughness and computation of depression storage. In Proceedings of the World Environmental and Water Resources Congress 2010: Challenges of Change, Providence, RI, USA, 16–20 May 2010; pp. 4437–4446.
35. Yang, J.; Chu, X.; Chi, Y.; Sande, L. Effects of rough surface slopes on surface depression storage. In Proceedings of the World Environmental and Water Resources Congress 2010: Challenges of Change, Providence, RI, USA, 16–20 May 2010; pp. 4427–4436.
36. Denmark's Digital Elevation Model. Available online: http://www.niras.com/Business-Areas/Mapping/Map-products/Denmarks-elevation-model.aspx (accessed on 1 September 2013).
37. Fakta om Laserskanning. Available online: http://www.lantmateriet.se/Kartor-och-geografisk-information/Hojddata/Fakta-om-laserskanning/ (accessed on 22 November 2013).
38. Pitkän aikavälin laserkeilaussuunnitelma kattaa kattaa vuodet 2014–2019. Available online: http://www.maanmittauslaitos.fi/kartat/laserkeilausaineistot/laserkeilausindeksit/laserkeilaussuunnitelma-2014–2019 (accessed on 1 September 2013).
39. Laser Scanning Data. Available online: http://www.maanmittauslaitos.fi/en/maps-5 (accessed on 1 September 2013).
40. Ullah, W.; Dickinson, W.T. Quantitative description of depression storage using a digital surface model. 1. Determination of depression storage. *J. Hydrol.* **1979**, *42*, 63–75.

41. Jenson, S.K.; Domingue, J.O. Extracting topographic structure from digital elevation data for geographic information-system analysis. *Photogramm. Eng. Remote Sens.* **1988**, *54*, 1593–1600.
42. Martz, L.W.; Garbrecht, J. The treatment of flat areas and depressions in automated drainage analysis of raster digital elevation models. *Hydrol. Process.* **1998**, *12*, 843–855.
43. Rieger, W. A phenomenon-based approach to upslope contributing area and depressions in DEMs. *Hydrol. Process.* **1998**, *12*, 857–872.
44. Freeman, T.G. Calculating catchment-area with divergent flow based on a regular grid. *Comput. Geosci.* **1991**, *17*, 413–422.
45. Planchon, O.; Darboux, F. A fast, simple and versatile algorithm to fill the depressions of digital elevation models. *Catena* **2002**, *46*, 159–176.
46. Ukkonen, T.; Sarjakoski, T.; Oksanen, J. Distributed computation of drainage basin delineations from uncertain digital elevation models. In Proceedings of the 15th Annual ACM International Symposium on Advances in Geographic Information Systems, Seattle, WA, USA, 7–9 November 2007; pp. 236–243.
47. Rieger, W. Automated river line and catchment area extraction from DEM data. *Int. Arch. Photogramm. Remote Sens.* **1993**, *29*, 642–642.
48. Lindsay, J.B.; Creed, I.F. Removal of artifact depressions from digital elevation models: Towards a minimum impact approach. *Hydrol. Process.* **2005**, *19*, 3113–3126.
49. Lindsay, J.B.; Creed, I.F. Distinguishing actual and artefact depressions in digital elevation data. *Comput. Geosci.* **2006**, *32*, 1192–1204.
50. Mansikkaniemi, H.; Seura, S.M. Sedimentation and water quality in the flood basin of the river Kyrönjoki in Finland. *Geogr. Soc. Finl.* **1985**, *163*, 155–194.
51. Flood Risk Management Planning in Finland. Available online: http://www.environment.fi/en-US/Water_and_sea/Floods/Flood_risk_management/Flood_risk_management_planning (accessed on 20 September 2013).
52. Saunders, W. Preparation of DEMs for Use in Environmental Modeling Analysis. In *Hydrologic and Hydraulic Modeling Support with Geographic Information Systems*; ESRI Press: New York, NY, USA, 2000; pp. 29–52.
53. Digital Elevation Model 2 m. Available online: http://www.maanmittauslaitos.fi/en/digituotteet/digital-elevation-model-2-m (accessed on 31 January 2013).
54. Laserkeilausaineisto. Available online: http://www.maanmittauslaitos.fi/digituotteet/laserkeilausaineisto (accessed on 31 January 2013).
55. Vilhomaa, J. Valtakunnallisen korkeusmallin tuotantoprosessin kehitystyö (Development of a production process for a national elevation model). Licentiate's Thesis, Aalto University, Espoo, Finland, 2008.
56. Korkeusmalliryhmä. *Valtakunnallisen korkeusmallin uudistamistarpeet ja -vaihtoehdot*; Ministry of Agriculture and Forestry: Helsinki, Finland, 2006; p. 76.
57. Korkeusmalli 10 m. Available online: http://www.maanmittauslaitos.fi/digituotteet/korkeusmalli-10-m (accessed on 31 January 2013).
58. Nash, J.; Sutcliffe, J. River flow forecasting through conceptual models Part I—A discussion of principles. *J. Hydrol.* **1970**, *10*, 282–290.

59. Moriasi, D.N.; Arnold, J.G.; Van Liew, M.W.; Bingner, R.L.; Harmel, R.D.; Veith, T.L. Model evaluation guidelines for systematic quantification of accuracy in watershed simulations. *Trans. ASABE* **2007**, *50*, 885–900.
60. French, J.R. Critical perspectives on the evaluation and optimization of complex numerical models of estuary hydrodynamics and sediment dynamics. *Earth Surf. Processes* **2010**, *35*, 174–189.
61. Lotsari, E.; Wainwright, D.; Corner, G.D.; Alho, P.; Käyhkö, J. Surveyed and modelled one-year morphodynamics in the braided lower Tana River. *Hydrol. Process.* **2014**, *28*, 2685–2716.
62. Suomen Salaojakeskus Oy. *Ilmajoen tulvariskien hallinnan yleissuunitelma*; Suomen Salaojakeskus Oy: Ilmajoki, Finland, 2010; p. 67.
63. American Society of Civil Engineers. Criteria for evaluation of watershed models. *J. Irrig. Drain. Eng. ASCE* **1993**, *119*, 429–442.
64. Legates, D.R.; McCabe, G.J. Evaluating the use of "goodness-of-fit" measures in hydrologic and hydroclimatic model validation. *Water Resour. Res.* **1999**, *35*, 233–241.
65. McCuen, R.H.; Knight, Z.; Cutter, A.G. Evaluation of the nash-sutcliffe efficiency index. *J. Hydrol. Eng.* **2006**, *11*, 597–602.
66. Ahokas, E.; Kaartinen, H.; Hyyppä, J. On the quality checking of the airborne laser scanningbased nationwide elevation model in Finland. *Int. Arch. Photogramm. Remote Sens. Spat. Inf. Sci.* **2008**, *37*, 267–270.
67. Kamphorst, E.C.; Jetten, V.; Guerif, J.; Pitkanen, J.; Iversen, B.V.; Douglas, J.T.; Paz, A. Predicting depressional storage from soil surface roughness. *Soil Sci. Soc. Am. J.* **2000**, *64*, 1749–1758.
68. Tribe, A. Automated recognition of valley lines and drainage networks from grid digital elevation models—A review and a new method. *J. Hydrol.* **1992**, *139*, 263–293.
69. Sane, M.; Alho, P.; Huokuna, M.; Käyhkö, J.; Selin, M. *Opas yleispiirteisen tulvavaarakartoituksen laatimiseen (Guidelines for flood hazard mapping on a coarse scale)*; Environment Guide 127; Finnish Environment Institute: Helsinki, Finland, 2006; p. 73.